



An integrated method for atherosclerotic carotid plaque segmentation in ultrasound image



Chunjun Qian^{a,*}, Xiaoping Yang^{a,b}

^aSchool of Science, Nanjing University of Science and Technology, Jiangsu, China

^bDepartment of Mathematics, Nanjing University, Jiangsu, China

ARTICLE INFO

Article history:

Received 10 March 2017

Revised 16 September 2017

Accepted 2 October 2017

Keywords:

Atherosclerotic carotid plaque
Semi-automatic plaque segmentation
Random forest
Auto-context model
Ultrasound Image

ABSTRACT

Background and objective: Carotid artery atherosclerosis is an important cause of stroke. Ultrasound imaging has been widely used in the diagnosis of atherosclerosis. Therefore, segmenting atherosclerotic carotid plaque in ultrasound image is an important task. Accurate plaque segmentation is helpful for the measurement of carotid plaque burden. In this paper, we propose and evaluate a novel learning-based integrated framework for plaque segmentation.

Methods: In our study, four different classification algorithms, along with the auto-context iterative algorithm, were employed to effectively integrate features from ultrasound images and later also the iteratively estimated and refined probability maps together for pixel-wise classification. The four classification algorithms were support vector machine with linear kernel, support vector machine with radial basis function kernel, AdaBoost and random forest. The plaque segmentation was implemented in the generated probability map. The performance of the four different learning-based plaque segmentation methods was tested on 29 B-mode ultrasound images. The evaluation indices for our proposed methods were consisted of sensitivity, specificity, Dice similarity coefficient, overlap index, error of area, absolute error of area, point-to-point distance, and Hausdorff point-to-point distance, along with the area under the ROC curve.

Results: The segmentation method integrated the random forest and an auto-context model obtained the best results (sensitivity $80.4 \pm 8.4\%$, specificity $96.5 \pm 2.0\%$, Dice similarity coefficient $81.0 \pm 4.1\%$, overlap index $68.3 \pm 5.8\%$, error of area $-1.02 \pm 18.3\%$, absolute error of area $14.7 \pm 10.9\%$, point-to-point distance 0.34 ± 0.10 mm, Hausdorff point-to-point distance 1.75 ± 1.02 mm, and area under the ROC curve 0.897), which were almost the best, compared with that from the existed methods.

Conclusions: Our proposed learning-based integrated framework investigated in this study could be useful for atherosclerotic carotid plaque segmentation, which will be helpful for the measurement of carotid plaque burden.

© 2017 Elsevier B.V. All rights reserved.

1. Introduction

The latest statistics from 2016 showed that stroke, a cardiovascular diseases, has become the fifth leading cause of death [1]. One of the important causes of stroke is atherosclerosis [2,3], which is a chronic disease. Atherosclerosis reduces the elasticity of the arterial walls and narrows the arteries [4], and it is characterized by plaque formation due to progressive intimal accumulation of lipids, protein, and cholesterol esters in the blood vessel wall [5]. Endarterectomy or stenting is the usual surgical procedure indicated by the stenosis of 70% or more [6]. However, many patients with large carotid plaque burden have no stenosis, i.e., carotid plaque

burden is not the same as stenosis, because of compensatory enlargement of arteries [7]. Non-invasive and low-cost ultrasound imaging has been widely used in the diagnosis of cardiovascular diseases [8,9], including atherosclerosis. Therefore, accurate segmentation of atherosclerotic carotid plaque in the ultrasound image with the assistance of computer is an important task, which is helpful for the measurement of carotid plaque burden. Plaque burden measurement is useful for risk stratification, determination of treatment plan, genetic research and assessment of the effects of new therapies on atherosclerosis [3,10,11].

There are many studies related to atherosclerotic carotid plaque segmentation in ultrasound images. Two types of ultrasound images are used for plaque segmentation in the presented studies. One is transverse ultrasound images. For example, Abolmaesumi et al. [12] presented a fully automatic tracking and segmentation

* Corresponding author.

E-mail addresses: qianchunjun@gmail.com, 611112283@njust.edu.cn (C. Qian).

system for extracting CCA boundaries from transverse ultrasound images in real time. In [13], a modified Star-Kalman approach was proposed by Guerrero et al. to determine vessel contours and ellipse parameters. Ukwatta et al. [14] described a 3D algorithm based on a modified sparse field level set algorithm to segment plaque, which yielded high-accuracy and high-repeatability. Aside from transverse ultrasound images, another type of ultrasound image used for plaque segmentation is longitudinal ultrasound image. Hamou et al. [15] proposed a method based on the histogram equalization and Canny edge detection algorithms to detect the plaque regions in longitudinal 2D CCA ultrasound images. Abdel-Dayen et al. [16] used a morphological approach for the carotid contour extraction from longitudinal ultrasound images of the CCA. Four different snake models (Balloon, gradient vector flow (GVF), Lai & Chin, William & Shah), with initialization based on Doppler blood flow images, were used and evaluated for segmenting plaque in longitudinal ultrasound images by Loizou et al [17].

In addition to the distinctions among the types of ultrasound images used in these presented studies, there is a difference in the automaticity of the existing methods. Among the aforementioned methods, some are semi-automatic, such as that in [14]. Indeed, in recent decades, many semi-automatic methods were validated for plaque segmentation. Gill et al. [18] proposed a semi-automatic segmentation method to track the progression of atherosclerotic plaque in three-dimensional (3D) images of the carotid artery by introducing the balloon model [19]. Cardinal et al. [20] used a semi-automatic intravascular ultrasound (IVUS) segmentation model to segment the lumen, intima-media thickness, and plaque in parallel with a fast-marching approach. A semi-automated method was proposed by Buchanan et al. [21] to measure the 3D ultrasound plaque. Destrempes et al. [22] segmented plaques in the sequences of B-mode ultrasound images using the Bayesian model combined with the manual starting point segmented in the first frame. They tested their proposed segmentation method on 94 sequences of 33 patients (for a total of 8988 images), and obtained a mean point-to-point distance of $0.24 \pm 0.08\text{mm}$, together with a Hausdorff distance of $1.24 \pm 0.40\text{mm}$.

Furthermore, automatic and robust segmentation of atherosclerotic carotid plaque in ultrasound images has attracted more researchers. Other than the methods presented in [12,17], other automatic algorithms were also proposed in succession. In [23], the Hough transform was applied to perform plaque segmentation in four 2D cross-sectional ultrasound images. Considering the complex structure and heterogeneity of plaques, Cheng et al. [24] introduced a fully automatic algorithm based on a hybrid level-set framework to outline carotid plaques in 3D ultrasound images by making use of the prior knowledge of the media adventitia boundary and lumen intima boundary. In [25], a fully automated methodology integrating the graphical models and Markov random fields was proposed to identify the plaque region by Gastounioti et al. In fact, ultrasound imaging techniques contain many other types, such as color Doppler, contrast-enhanced ultrasound (CEUS), and so on [26]. In [17], researchers established initialization on color Doppler blood flow images. Akkus et al. [27] were the first to introduce the method for carotid plaque segmentation by exploiting the combined information from simultaneously acquired B-mode ultrasound and CEUS images. Their proposed method comprised several processing parts that contained non-rigid motion estimation and compensation, vessel detection, and plaque segmentation.

In a word, the superiority of ultrasound imaging rests in the computer-aided diagnosis (CAD) of carotid plaque; however, ultrasound B-mode imaging presents several difficulties due to some typical image characteristics, such as low contrast, speckle noise, echo shadows and artifacts, which usually leads to poor quality images that require the interpretation of an expert [8]. As described

in [28], speckle is a multiplicative noise in ultrasound imaging. If the mathematical models (i.e., snake model [17], level set [14,24], and balloon model [18,19]) are used for plaque segmentation, a denoising algorithm is necessary, which requires prior knowledge regarding the type of the speckle noise, the distribution of the speckle noise, etc. Fortunately, learning-based algorithms can be robustly used for the images with noise and artifacts, et al [29,30].

Although most of the proposed atherosclerotic carotid plaque segmentation methods have achieved satisfactory performance, there are some limitations and areas for improvement. (1) Some articles describe carotid segmentation techniques only of the walls and not of the plaque itself [12,13,16,18,23]. (2) A few existing methods require careful initialization, and often require careful parameter tuning for convergence [14,17,24]. (3) Some of the proposed methods, especially semi-automatic methods, require a certain amount of manual operations, which introduce operator variability [21,22]. (4) In [17,27], the fully automatic plaque segmentation methods, combining different modalities of ultrasound image, are presented. These methods require that the imaging devices record the different modalities of ultrasound images simultaneously, or the image registration techniques are employed between different modalities of images.

To overcome the difficulties inherent in ultrasound images and to improve the limitations of the existing methods, in this paper, we introduce an integrated framework to semi-automatically segment atherosclerotic carotid plaque in the B-mode longitudinal ultrasound image. Our proposed method, integrating learning-based algorithms and an auto-context model [31,32], consists of region of interest (ROI) extraction, plaque ROI candidate identification and plaque segmentation. We have validated our proposed method on 29 patient subjects and obtained promising performance.

2. Database

In our work, all the data are open resource and were made available by Loizou et al. [17,28] on the social networking site Research Gate. For the convenience of the reader, we describe the database repeatedly.

2.1. Dataset introduction

The database contains a total of 80 B-mode and blood flow longitudinal ultrasound images of the CCA, the normalized images of the atherosclerotic carotid plaques and the manual delineated images, as well as Doppler color ultrasound images (which are not used in our method). Only 29 patient subjects can be used in our study, however, due to the presence of duplicate images, which may be the result of the loss of other images in the transmission or storage process. All the images were acquired using an ATL HDI-3000 ultrasound scanner (Advanced Technology Laboratories, Seattle, USA) and were recorded digitally on a magneto optical drive with a resolution of 768×576 pixels with 256 Gy levels. Digital images were resolution-normalized at 16.66 pixels/mm (see Section II-C in [17]). The images were recorded at Saint Mary's Hospital, Imperial College of Medicine, Science and Technology, U.K., from 29 symptomatic patients. These patients were at risk of atherosclerosis and had already developed clinical symptoms such as a stroke or a transient ischemic attack. The degree of carotid artery stenosis of the interrogated subjects was $50.59 \pm 21.26\%$ with the North American Symptomatic Carotid Endarterectomy Trial (NASCET) formula ($r = (1 - D_1/D_2) \times 100$) or $66.81 \pm 11.91\%$ by the European Carotid Surgery Trial (ECST) formula ($r = (1 - D_1/D_3) \times 100$). r represents the degree of carotid artery stenosis. D_1 is the narrowest internal carotid artery (ICA) diameter, and D_2 diameter normal distal cervical ICA. The estimated original diameter at the site of the stenosis is denoted as D_3 [33].

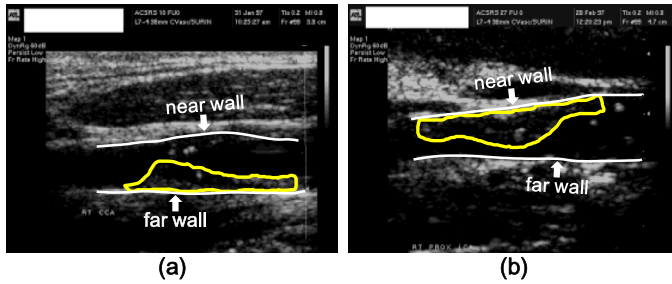


Fig. 1. Two different plaques are attached to (a) the far wall and (b) the near wall of the blood vessel, respectively. The white curves indicate the walls of blood vessel, and the yellow curve indicates the contour of the plaque delineated by the expert. (For interpretation of the references to color in this figure legend, the reader is referred to the web version of this article.)

In these images, different types of atherosclerotic plaque with irregular geometric appearances can be observed in the blood vessel. Each of the B-mode ultrasound images was selected randomly, together with the blood flow longitudinal ultrasound image. In our study, only B-mode ultrasound images are regarded as source images. Incidentally, manual delineated images are used as ground truth. In fact, in our study, we do not use the blood flow longitudinal ultrasound images and normalized images. The characteristics of normalized image change too much compared with the original B-mode ultrasound image. The registration between B-mode ultrasound image and blood flow longitudinal ultrasound image is challenging, and there is no expert to evaluate the performance of registration. In particular, our proposed method does not need any initialization, but Loizou et al. [17] extracted the boundary of blood flow region from the blood flow longitudinal ultrasound image as the initial snake contour.

The ground truth of plaque was generated as follows. An expert manually delineated the plaque borders between plaque and the artery wall, and the borders between plaque and blood, on 29 B-mode ultrasound images of the carotid artery after image normalization and speckle reduction filtering (see Section II-C and II-D in [17]) using MATLAB software developed by other researchers from the group of Loizou et al. The manual delineation process was established by a team of experts and was documented in the ACSRS

project protocol [34]. The correctness of the work carried out by a single expert was monitored and verified by at least one other expert. To the best of our knowledge, as documented in [34,35], the plaques can be classified from type I to type V. In this study, considering the ease of making manual delineations, only the plaques of type II, III, and IV were outlined because the fibrous cap, which is the border between blood and plaque, renders them more easily identified. If the plaque is of type I, borders are not properly visible. Plaques of type V produce acoustic shadowing and the plaque is also not properly visible.

2.2. Ground truth of blood vessel

To apply the learning-based method effectively in our work, we label the blood region manually by a non-medical approach because of the lack of a special image reader. It is commonly known that ultrasound images like those shown in Fig. 1 are difficult to read without any training, and it is challenging to directly identify the boundaries or near wall/far wall of the vascular (blood region mentioned in Section 3.1). In our study, however, the manually labeled blood region should only cover the plaque area completely. Considering this property of the labeled blood vessel, we manually outline it according to the contour of the plaque. The contour of the blood vessel is made up of two white lines. One line indicates the near wall and the other one is the far wall of vascular, and the area between the two such lines regarded as the blood region covers the plaque completely, as shown in Fig. 1. Fig. 1 shows two examples of plaques attached to the far wall (Fig. 1(a)) or the near wall (Fig. 1(b)). The white curves are the approximate boundaries of the blood vessel and yellow lines indicate the contour of plaque as defined by the expert.

3. Proposed method

Our proposed method consists of three processing steps, as shown in Fig. 2. (1) The first step is aimed at preprocessing the ultrasound image and extracting ROI from the whole ultrasound image. (2) The second step concerns plaque region candidate identification. More importantly, the extracted candidate should absolutely cover the plaque. (3) The third step is the segmentation of the carotid plaque in the classification map, which is generated by

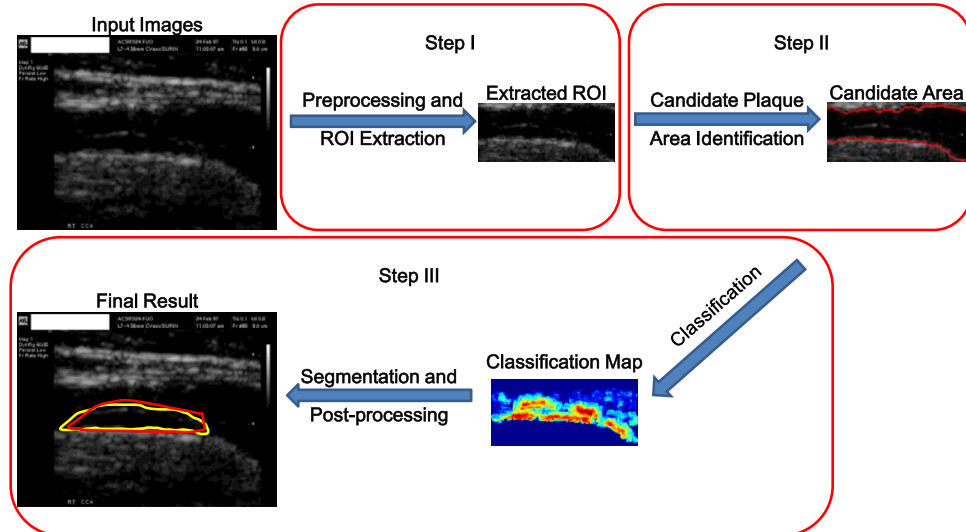


Fig. 2. Flowchart of our proposed method. Our method is composed of three major steps: (1) Ultrasound image preprocessing and ROI extraction, (2) Candidate plaque ROI identification, and (3) Plaque segmentation. In Step II, the extracted candidate plaque region is contoured by red curves. In the final result, the red curve indicates the plaque contour by our proposed method and the yellow curve is the ground truth delineated by the expert. (For interpretation of the references to color in this figure legend, the reader is referred to the web version of this article.)

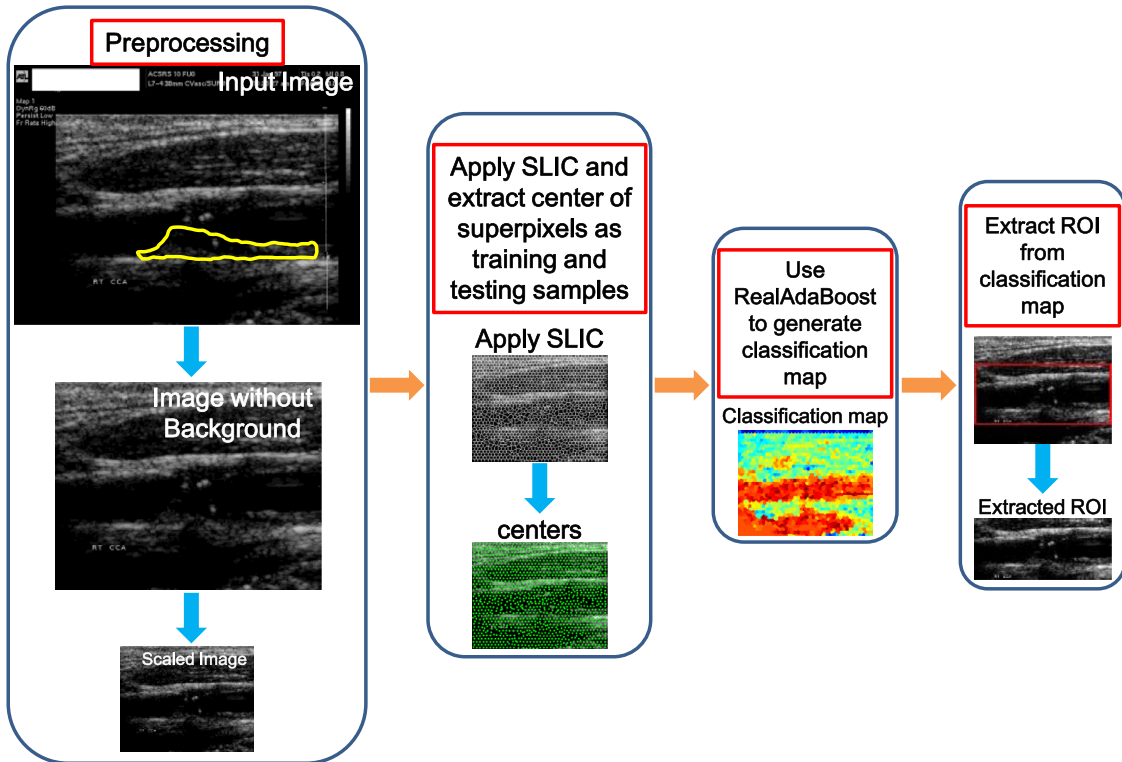


Fig. 3. Flowchart of Step I in our method. ROI is extracted through scaling the image and applying classification algorithm, and ROI is contoured by a window with a height of 130 pixels and the original width of the scaled image. (For interpretation of the references to color in this figure legend, the reader is referred to the web version of this article.)

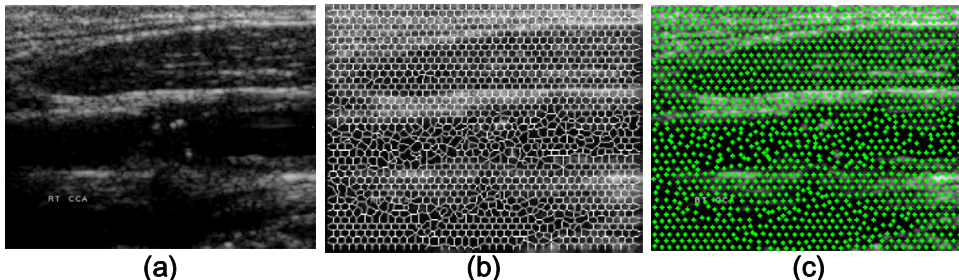


Fig. 4. Ultrasound image is segmented into superpixels by using SLIC. (a) Original image, (b) The result of superpixel segmentation, (c) The centers of superpixels (green dots). (For interpretation of the references to color in this figure legend, the reader is referred to the web version of this article.)

the learning-based method. We will describe our method step by step in detail in the following subsections.

3.1. Ultrasound image preprocessing and ROI extraction

First, as shown in Fig. 3, we remove the background because its characteristics are similar to that of the blood area. In our work, the ROI extraction is mainly based on the characterization of blood area. The blood area and plaque area are wrapped by the vascular walls. Taking the computational burden and cost into consideration, we scale the image to quarter size.

To implement ROI extraction automatically, we apply the learning-based algorithm together with superpixel algorithm. The superpixel algorithm locally groups pixels into perceptually meaningful atomic regions that can be used to replace the rigid structure of the pixel grid [36]. Specifically, we use the simple linear iterative clustering (SLIC) algorithm (one of the superpixel algorithms) [37] to oversegment the images into approximately 1500 superpixels, and the SLIC can produce superpixels with a lower computational cost while achieving a satisfactory oversegmentation result. In the following learning-based ROI extrac-

tion, we extract the centers (the green dots as shown in Fig. 4) of the superpixels as the training or testing samples.

Subsequently, the RealAdaBoost in AdaBoost [38] tool is employed as the classifier to generate the classification map. Here, the extracted centers in the manually labeled blood region are treated as positive samples and other centers are negative samples. To the best of our knowledge, the CCA lumen diameter ranges from 4.6 mm to 6.6 mm [39,40]. Therefore, with the imaging equipment information mentioned in [17,28], the maximum lumen diameter is approximately 110 pixels in the scaled image (approximately 220 pixels in the original image). In the database, all the plaques are attached to the far wall or near wall of the vascular (as shown in Fig. 1), and only one plaque area is delineated in each of the images. Finally, we set the height of window as 130 pixels and the width of window as equal to the scaled image to extract ROI.

3.2. Candidate plaque area identification

There are many interfering factors for directly segmenting plaque in the extracted image of ROI shown in the fourth column of Fig. 3. From extracted ROI image in Fig. 3, as well as the im-

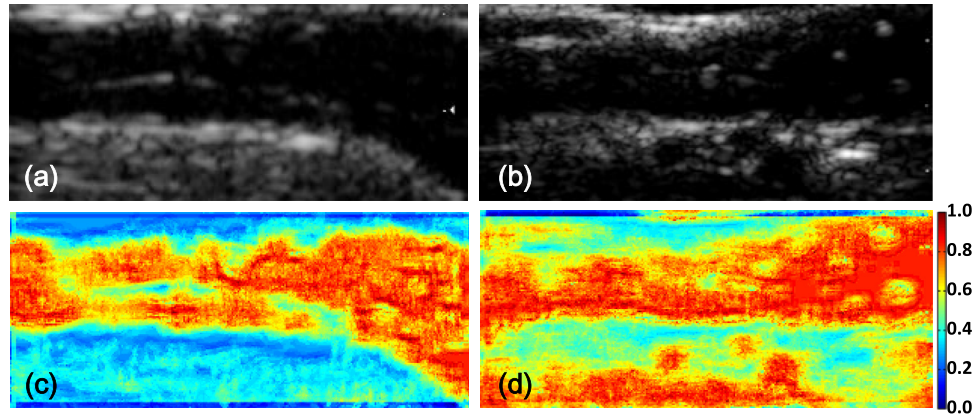


Fig. 5. Classification maps of two extracted ROI images. (a), (b): Two extracted ROI images; (c), (d): Probability maps of two examples. (For interpretation of the references to color in this figure legend, the reader is referred to the web version of this article.)

ages in Fig. 1, it can be observed that some bright spots in the plaque area delineated by yellow curve are similar to those out of the blood vessel, and the characterization of the vascular region except the plaque area is similar to that of some other areas in the B-mode ultrasound image. In other words, these interfering factors greatly affect the performance of the classifier, which ultimately leads to inaccurate carotid plaque segmentation. Therefore, to reduce these interfering factors, automatic plaque ROI candidate identification based on the machine learning method is adopted in our method.

In fact, the procedure of candidate plaque region identification is not overly complex. It can be formulated as the two-class classification problem. Together with the manually labeled map of the blood vessel, the training ultrasound images are put into the classifier, and then the trained classification model is obtained. For a new image, the model is used to identify the candidate plaque area. The automatic candidate plaque area identification in the extracted ROI image can be implemented through a variety of learning-based methods, such as AdaBoost, SVM [41,42] or random forest [43], etc. Fig. 5 shows classification maps (automatically generated by the learning-based method) of two examples. In the classification maps (Fig. 5(c) and (d)), there is a probability value to represent each pixel as residing (or not) in a candidate plaque area. As seen from the colorbar in Fig. 5, the candidate plaque areas are consisted of the pixels whose probability values are over 0.7 refer to the extracted ROI images in Fig. 5(a) and (b). Therefore, we can obtain the desired results in Fig. 5(c) and (d) by a simple threshold-based segmentation algorithm, together with maximally connected components and morphological operation algorithms.

3.3. Plaque segmentation

After ultrasound image preprocessing and candidate plaque area identification, we achieve the atherosclerotic carotid plaque segmentation in Step III. We find that most of the interfering regions, which are similar to the plaque area, are removed in the image of candidate plaque generated in Step II. This is helpful to obtain the expected segmentation result in the image of candidate plaque with the learning-based algorithm.

Here, we formulate the task of plaque segmentation from the image of candidate plaque as a two-class classification problem, i.e., in our work, we look upon the pixels in the plaque area as the positive samples and those in the candidate plaque regions but outside the plaque area as the negative ones. To solve this kind of classification problem, the learning-based algorithm is employed in the procedure of plaque segmentation. In the training stage, from the images as training set, a quantity of pixels from plaque and non-plaque regions are selected randomly as training

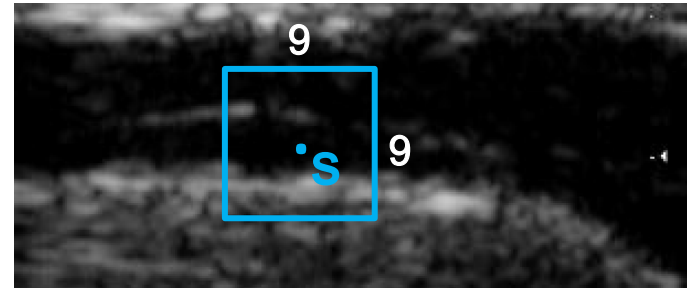


Fig. 6. Feature representation of the sample s in our method. The blue dot is denoted as s , which is the center of the 9×9 window. The blue curve indicates the feature extraction window. (For interpretation of the references to color in this figure legend, the reader is referred to the web version of this article.)

samples. Subsequently, combining the feature representations of the training samples, we train the classifier and obtain the training model. In the application stage, each pixel in the new image is regarded as testing sample and distinguished as positive or negative through applying the training model. Then, the probability map of the testing image can be obtained. Finally, we can obtain the segmentation result in the generated probability map by using some post-processing algorithms, such as threshold-based segmentation algorithm and morphological operation.

3.3.1. Feature representation

In our implementation, considering the efficiency and computational cost and speed, we use the simple intensity values of pixels around the training or testing sample as the feature representations from both gray-level image and iteratively estimated classification map (see section Auto-context Model). As shown in Fig. 6, the blue dot denoted as s represents a sample in the training or testing image. The blue curve indicates a feature extraction window with the size of 9×9 , and the center of the window is the sample s . All the gray values of pixels in the window are extracted as features for representing the sample s . Therefore, in all of three steps of our method, only 81 gray values are extracted as the features from grey-level images or iteratively estimated classification map, which greatly reduces the computing time while ensuring the independence and usefulness of the extracted features for each individual sample. This also ensures the performance of our plaque segmentation method.

3.3.2. Classification algorithm

In Step III of our proposed method, we use four different classification algorithms to segment the atherosclerotic carotid plaque

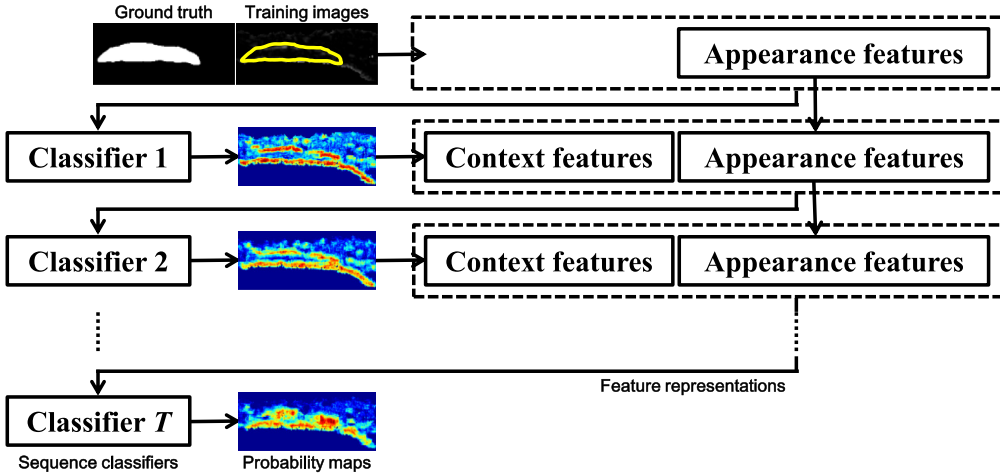


Fig. 7. Illustration of the training procedure for plaque segmentation with auto-context model. The appearance features from training images are used for training the first classifier, and then both appearance features from training images and context features from probability maps are employed for training the subsequent classifiers. (For interpretation of the references to color in this figure legend, the reader is referred to the web version of this article.)

and compare their performances on the same dataset. The classification algorithms adopted in our work include: (1) Support vector machine (SVM) with linear kernel (linear SVM) [41], (2) SVM with RBF kernel (SVM + RBF) [42], (3) AdaBoost [38], and (4) random forest [43].

- Support vector machine (SVM) is a supervised learning model associated with learning algorithms that analyze data and recognize patterns, which can be used for classification and regression. It is often used for solving a two-class classification problem. Given a set of training samples, each belonging to one of the two categories, an SVM training algorithm builds a model, i.e., generating two optimal hyperplanes to separate the input samples into two categories and preventing the samples from falling into the maximum margin (i.e., the gap between the hyperplanes). In our work, we choose the linear function and RBF kernel as two candidate kernel functions. The learning model is generated by training the input training samples with parameter settings, such as cost function (c) and gamma (g) in RBF kernel. In the application (testing) stage, the generated model is used for pixel-wise prediction in the testing image.
- AdaBoost has been a mature and popular machine learning algorithm for classification for decades. When training the input samples, it generates a series of weak learners by updating the weight on each training sample. In each iteration, a weak learner is selected and assigned with a coefficient such that the sum of training error of the boosting classifiers is minimized. After a certain number of iterations (i), the weak learners finally converge to a strong learner. Finally, the trained classifier is used in the testing stage and then the tissue probability map is obtained.
- Random forest is an ensemble learning method for classification or regression. As a machine learning method, it has been successfully applied in many fields, including bioinformatics, computer vision, and medical image analysis [44,45]. When the random forest classifier is implemented, totally M decision trees are used as classification trees. In the training stage, each tree learns a weak class predictor using features extracted from a set of training subjects. When the training stage starts, according to the feature representations, the training samples are assigned to the left and right child nodes at each parent node through recursive splitting. The tree keeps growing until it reaches the constraint conditions, e.g., the criterion that no tree leaf node should contain less than a certain number of training

Table 1

Parameter settings of the four different classification algorithms.

Classification method	c	g
linear SVM	1	–
SVM + RBF	1	$1/k$
AdaBoost	i	100
random forest	M	l
	300	8
		v
		40

samples (l). We also consider another parameter, i.e., the number of feature representations (v) randomly sampled as candidates at each split, in the training procedure. Then, the random forest classifier can be obtained by training the input samples with the extracted features. Subsequently, in the testing stage, an unknown subject is tested by applying the generated random forest model.

3.3.3. Auto-context model

To improve the plaque segmentation, also inspired by Wang's study of segmentation of infant brain images [46] and our previous work on prostate cancer localization [47], we reintroduce the auto-context model [31,32] in the current work on plaque segmentation. The training stage and testing stage are almost similar, and the flowchart of the training stage is shown in Fig. 7.

For simplicity, let N be the total number of training images and let $I = \{I_n, n=1, \dots, N\}$ be a set of training images. Let $t = 1, \dots, T$ be the number of iterations. In the training stage, we will train a sequence of classifiers, each with the input of training images/probability maps. In the first iteration, the classifier takes only the training images I as input and uses the image appearance features for pixel-wise classification. By applying the trained classifier in the first iteration, each n th training image will produce the plaque probability map P_n^1 , as shown in the second row of Fig. 7. In the later iterations, as inspired by the auto-context model, the probability maps $\{P_n^t, n=1, \dots, N, t=2, \dots, T-1\}$ obtained from the previous iteration will act as additional source information for training. Specifically, the high-level context features extracted from the probability maps can assist the classification, along with the appearance features. Because context features are informative about the nearby tissue structures for each pixel, they encode the spatial constraints into the classification, thus improving the quality of the estimated probability maps, as also demonstrated in Fig. 7. Then, the plaque probability maps are iteratively

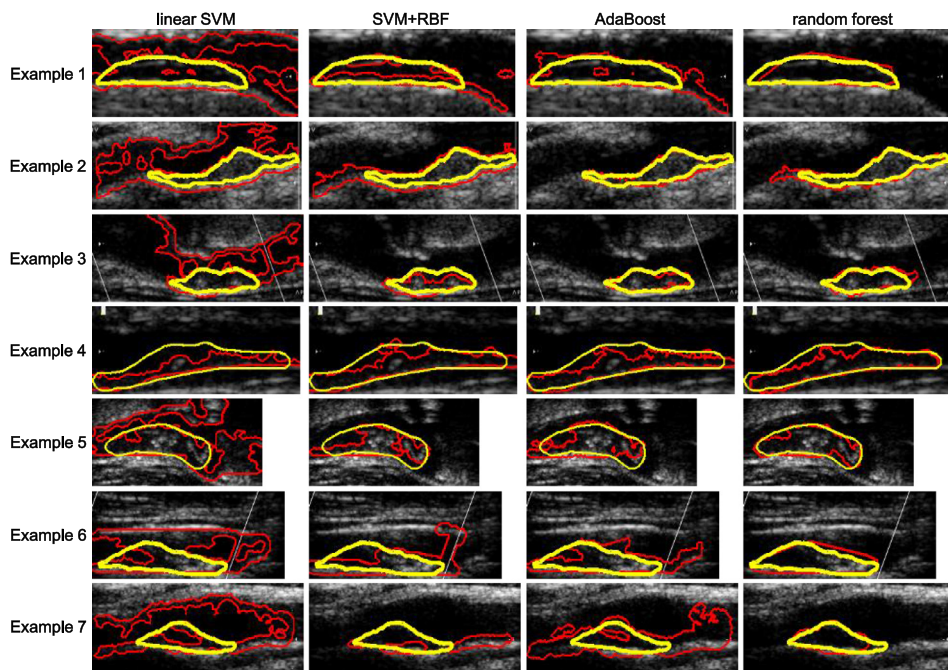


Fig. 8. Examples of plaque segmentation by using proposed method with different classification algorithms. The yellow curve represents the boundary of manual segmentation by the expert, i.e., ground truth. The red curve indicates the boundary of plaque segmented by the proposed method. (For interpretation of the references to color in this figure legend, the reader is referred to the web version of this article.)

Table 2

Performance metrics of sensitivity (true-positive rate, TPR), specificity (true-negative rate, TNR), Dice similarity coefficient (DSC), and overlap index for the atherosclerotic carotid plaque segmentation methods performed on the database.

Study	Number of images	Segmentation method	Sensitivity (TPR) (%)	Specificity (TNR) (%)	DSC (%)	Overlap index (%)	Automatic or semi-automatic
Loizou et al. [17]	80	Williams & Shah	81.8	93.5	78.9	67.6	Automatic
		Balloon	80.4	94.6	77.9	67.8	Automatic
		Lai & Chin	82.7	94.2	80.7	69.3	Automatic
		GVF	79.6	93.7	77.3	66.6	Automatic
Golemati et al. [23]	4	Hough transform (systole)	97.5 ± 1.0	95.5 ± 1.0	—	—	Automatic
		Hough transform (diastole)	95.0 ± 4.1	97.3 ± 2.4	—	—	Automatic
Destrempe et al. [22] Proposed methods	8988 29	Bayesian model	83.7 ± 8.3	94.1 ± 4.2	84.8 ± 7.5	74.6 ± 10.1	Semi-automatic
		linear SVM	83.0 ± 14.4	80.5 ± 13.6	60.7 ± 12.9	44.9 ± 13.9	Semi-automatic
		SVM + RBF	76.8 ± 17.0	85.4 ± 12.5	62.4 ± 11.3	46.4 ± 12.0	Semi-automatic
		AdaBoost	77.2 ± 15.8	93.4 ± 4.7	71.8 ± 11.2	57.1 ± 13.1	Semi-automatic
		random forest	80.4 ± 8.4	96.5 ± 2.0	81.0 ± 4.1	68.3 ± 5.8	Semi-automatic

Table 3

Performance metrics of EArea, AEArea, point-to-point distance (D), and Hausdorff point-to-point distance (HD) for the atherosclerotic carotid plaque segmentation methods performed on the database.

Study	Number of images	Segmentation method	EArea (%) (plaque)	AEArea (%) (plaque)	D (mm)	HD (mm)
Destrempe et al. [22]	8988	Bayesian model	−2.52 ± 7.97	7.07 ± 4.99	0.24 ± 0.08	1.24 ± 0.40
Proposed methods	29	linear SVM	−89.3 ± 87.2	97.6 ± 77.9	1.12 ± 0.54	4.05 ± 1.57
		SVM + RBF	−49.0 ± 62.5	62.2 ± 49.3	0.97 ± 0.38	3.67 ± 1.13
		AdaBoost	−17.0 ± 51.4	36.8 ± 39.7	0.59 ± 0.37	3.20 ± 1.97
		random forest	−1.02 ± 18.3	14.7 ± 10.9	0.34 ± 0.10	1.75 ± 1.02

updated and fed into the next training iteration. Finally, a sequence of learned classifiers will be obtained.

Similarly, in the testing stage, given a testing image I_{test} , we can obtain the initial plaque probability map P_{test}^1 by applying the trained classifier in the first iteration. In the later iterations, along with the testing image, the plaque probability maps $\{P_{test}^t, t = 2, \dots, T - 1\}$ resulting from the previous iteration are also fed into the next classifier for refinement.

4. Experimental results and analysis

In this section, the proposed method will be extensively evaluated on the database made available by Loizou et al. [17,28] using

leave-one-out cross-validation. The results of the proposed method are compared with the manual ground-truth segmentations, as well as other state-of-the-art methods.

4.1. Parameter settings

In our work, we used four different classification algorithms and set the parameters of each kind of classification algorithm, as in Table 1. The cost functions (c) of both SVM with linear kernel and RBF kernel are set as 1, and the parameter gamma (g) of RBF kernel is set as $1/k$, where k is the number of training samples. When using the AdaBoost classification method, we set the maximum number of iterations (i) as 100 in the weak learner refin-

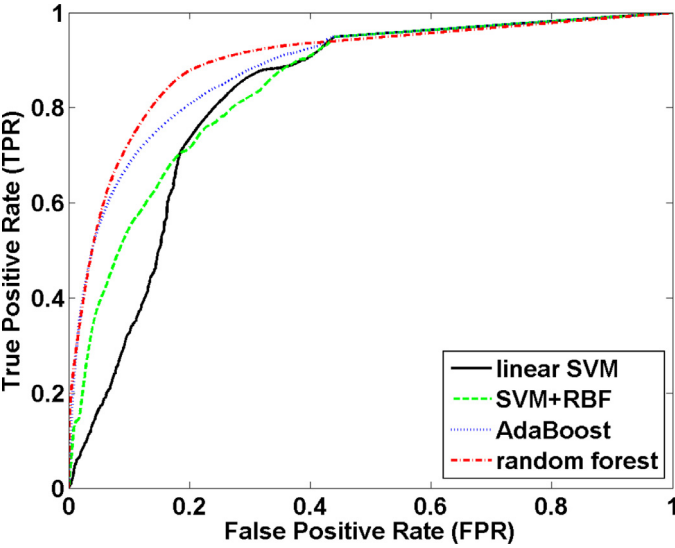
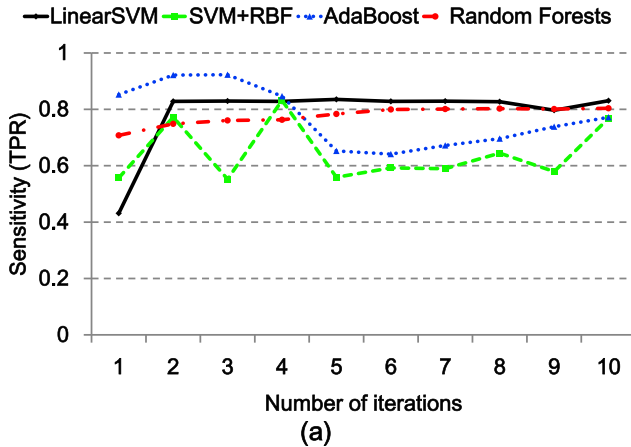
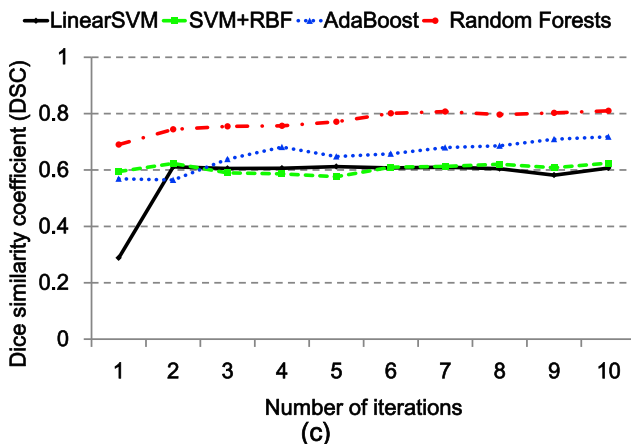


Fig. 9. ROC curves based on the TPR and FPR for the proposed method with the four different classification algorithms: linear SVM, SVM + RBF, AdaBoost, and random forest. (For interpretation of the references to color in this figure legend, the reader is referred to the web version of this article.)

ing process to build a strong classifier. To create a random forest model, a total of 300 decision trees are used. In addition, the minimum samples for each leaf node are set to 8 and 40 feature variables (v) are randomly sampled as candidates at each split.



(a)



(c)

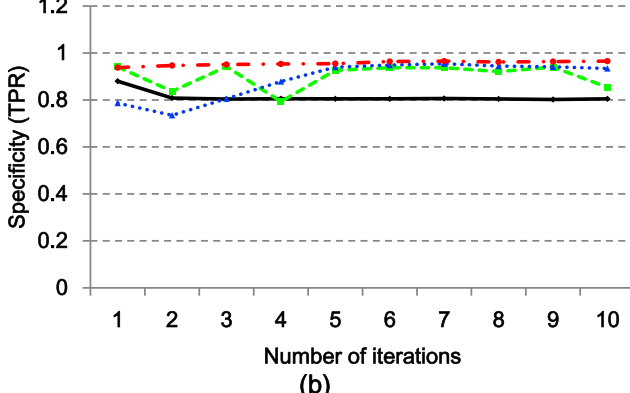
4.2. Evaluation methods

The receiver operating characteristic (ROC) analysis [48] is used to assess the sensitivity and specificity of the proposed atherosclerotic carotid plaque segmentation methods by true-positive rate (TPR) and true-negative rate (TNR). The TPR, also called sensitivity, is calculated when the sample is in the plaque area, and the computerized method identifies it. The true-negative rate (TNR), also called specificity, is calculated when the sample is not a plaque pixel and the computerized method identifies it as such (absent). Ratios of overlapping areas can also be assessed by measuring the Dice similarity coefficient (DSC) [49] and the overlap index [17]. These indices can be computed as:

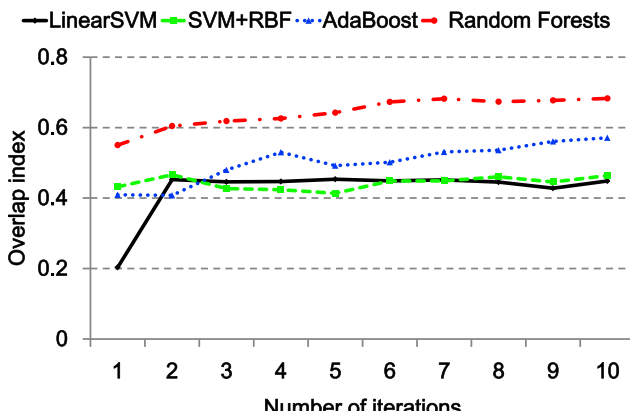
$$\begin{aligned} \text{TPR} &= \frac{|AS \cap GT|}{|GT|}, \quad \text{TNR} = \frac{|\overline{AS} \cap \overline{GT}|}{|\overline{GT}|}, \\ \text{DSC} &= 2 \frac{|GT \cap AS|}{|GT| + |AS|}, \quad \text{and overlap} = \frac{|GT \cap AS|}{|GT \cup AS|} \end{aligned} \quad (1)$$

where $|\cdot|$ denotes the magnitude, \cap denotes the intersection (the number of common pixels in the manually delineated plaque area and the segmented plaque area by the proposed method), and \cup is the union (the number of all pixels defined by the manual approach and the proposed method segmented plaque areas, where the common pixels are considered only once). GT is the number of pixels defined in the plaque area, representing ground truth delineated by the expert, and \overline{GT} is its complement. AS is the number of pixels in the segmented plaque area with proposed method and \overline{AS} is its complement. The intersection gives the probability that both AS and GT occur, and the union is the probability that either AS or GT occurs.

—LinearSVM —SVM+RBF —AdaBoost —Random Forests



(b)



(d)

Fig. 10. Improvements of the (a) sensitivity (TPR), (b) specificity (TNR), (c) DSC, and (d) overlap index, with iterations by using the four different classification algorithms. (For interpretation of the references to color in this figure legend, the reader is referred to the web version of this article.)

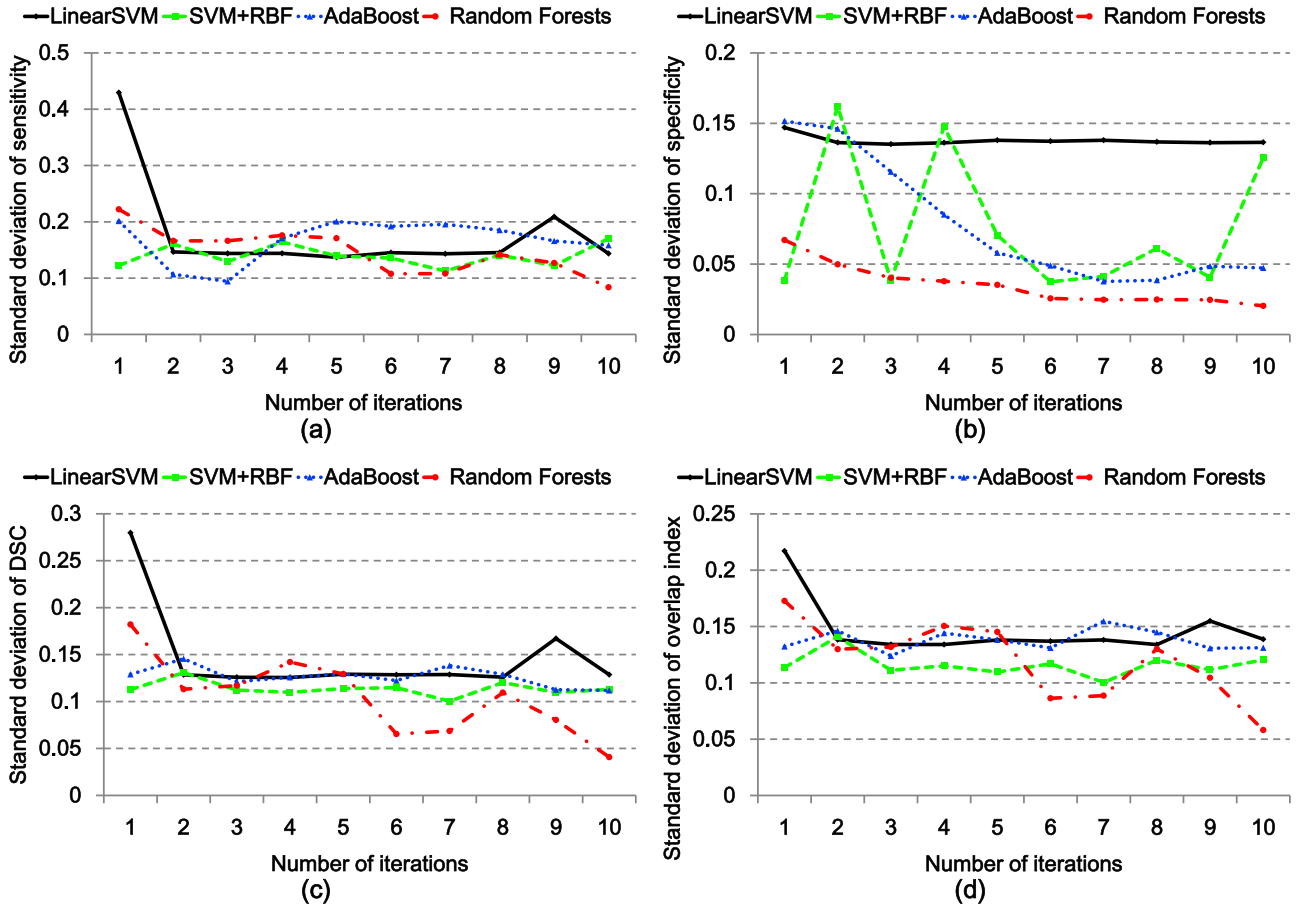


Fig. 11. Changes in the standard deviations of the (a) sensitivity, (b) specificity, (c) DSC, and (d) overlap index, with iterations, respectively. (For interpretation of the references to color in this figure legend, the reader is referred to the web version of this article.)

We also consider four measures of discrepancy, which are also used in [22]. The first two are the error of area (EArea) [13], and the absolute error of area (AEArea) [50]. Another two measures of discrepancy are based on the average point-to-point distance (D) and the Hausdorff point-to-point distance (HD), respectively [51], between the boundary of the region AS_R and that of the region GT_R . These four measures can be formulated as:

$$\begin{aligned} \text{EArea} &= \frac{|AS_R| - |GT_R|}{|GT_R|}, \quad \text{AEArea} = \frac{||AS_R| - |GT_R||}{|GT_R|}, \\ D(\partial AS_R, \partial GT_R) &= \text{average}_{a \in \partial AS_R} \min_{b \in \partial GT_R} \|a - b\|, \text{ and} \\ HD(\partial AS_R, \partial GT_R) &= \max(h(\partial AS_R, \partial GT_R), h(\partial GT_R, \partial AS_R)) \end{aligned} \quad (2)$$

where ∂AS_R and ∂GT_R denote the boundary of region AS_R and that of the region GT_R , respectively. $h(\partial AS_R, \partial GT_R) = \max_{a \in \partial AS_R} \min_{b \in \partial GT_R} \|a - b\|$, and $\|a - b\|$ is the Euclidean norm between points a and b . If HD is the Hausdorff distance between two sets AS_R and GT_R , then every point of AS_R must be within a distance HD of GT_R and vice versa [51].

4.3. Experimental results

To illustrate the effectiveness of our proposed method, that is, to demonstrate that the proposed method can effectively segment atherosclerotic carotid plaque in B-mode ultrasound images, we carry out the experiments on the database. All the experiments are implemented with MATLAB R2014a on a PC with 2.67 GHz Intel Xeon 12 CPU, RAM 16.00 G.

4.3.1. Examples of plaque segmentation with proposed method

In Figs. 8, 7 examples of plaque segmentation with the proposed method are shown. The yellow curve is the boundary of manual segmentation by the expert, i.e., ground truth. The red curve indicates the boundary of plaque segmented by the proposed learning-based method, which integrates the four different classification algorithms. Each row shows an example. The four different classification algorithms in our method are linear SVM, SVM + RBF, AdaBoost, and random forest respectively, from left to right in the column of each example. As illustrated in Fig. 8, both the manual and our random forest-based segmentation contours are visually quite similar. For example 3 and example 4, the segmentation results from using SVM + RBF, AdaBoost and random forest are almost the same, and are also much better than the results from linear SVM. For other examples shown in Fig. 8, the contours with random forest are almost similar to the ground truth, but this is not the case with the other three algorithms, except for that of example 2 by AdaBoost.

4.3.2. Evaluation of proposed method

Table 2 tabulates the results of the ROC analysis based on sensitivity (TPR), specificity (TNR), DSC, and overlap index, for the proposed plaque segmentation methods on 29 B-mode ultrasound images, along with that of other state-of-the-art methods in other studies. Specifically, the results with random forest are higher than those from any of the other three learning-based methods used in our proposed methods, except for the sensitivity. The sensitivity by random forest ($80.4 \pm 8.4\%$) is smaller than that by linear SVM ($83.0 \pm 14.4\%$), but still much better than that by SVM + RBF ($76.8 \pm 17.0\%$) and AdaBoost ($77.2 \pm 15.8\%$). Our proposed method,

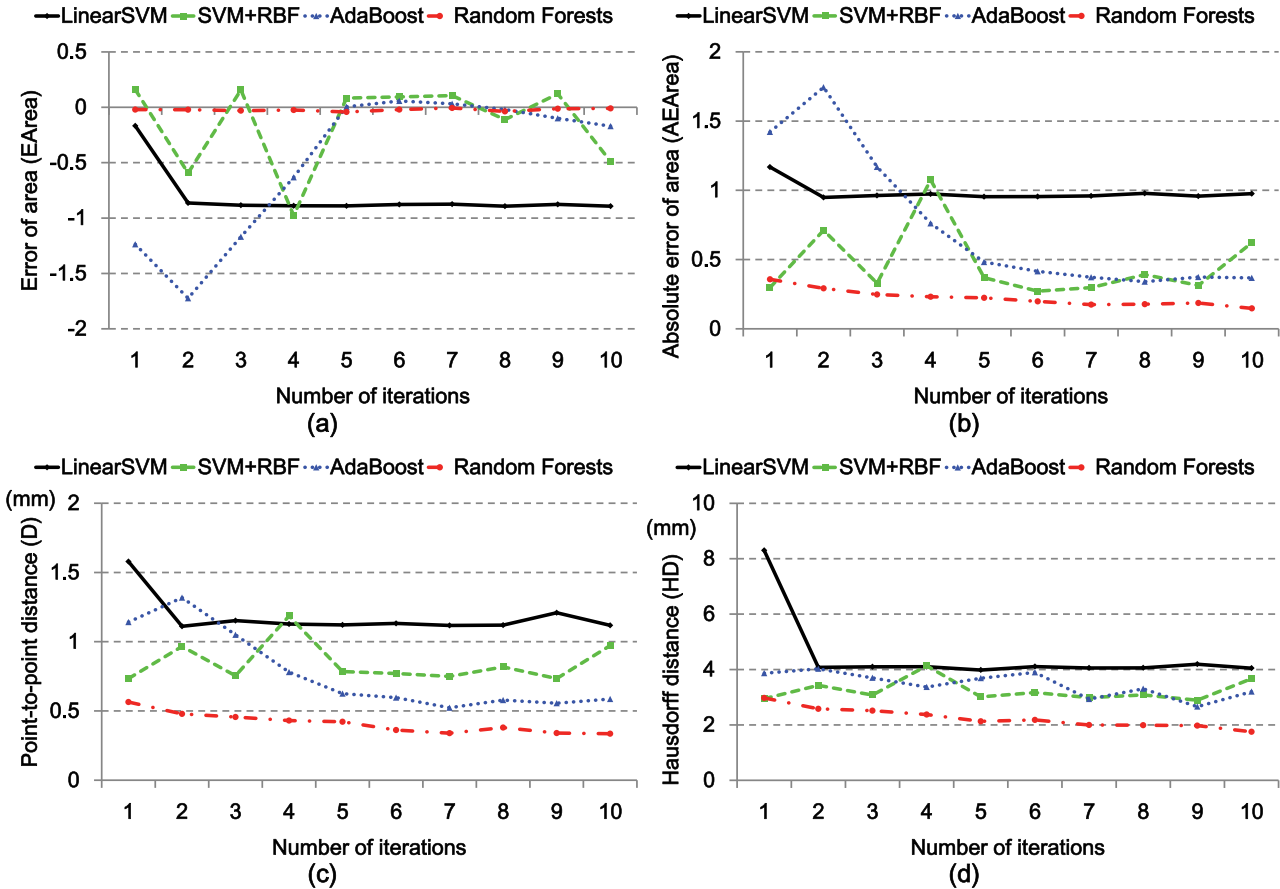


Fig. 12. Improvements of the (a) EArea, (b) AEArea, (c) point-to-point distance (D), and (d) Hausdorff distance (HD), with auto-context iterations. (For interpretation of the references to color in this figure legend, the reader is referred to the web version of this article.)

integrating the random forest algorithm, agrees with the expert by correctly detecting no plaque (TNR) in $96.5 \pm 2.0\%$ of the cases, which is much higher than those by linear SVM ($80.5 \pm 13.6\%$), SVM + RBF ($85.4 \pm 12.5\%$) and AdaBoost ($93.4 \pm 4.7\%$). The DSC and the overlap index for the random forest algorithm in our proposed methods are the highest, equal to $81.0 \pm 4.1\%$ and $68.3 \pm 5.8\%$, respectively. In other words, in the view of the DSC and overlap index, the performance of random forest is significantly better than that of linear SVM (DSC $60.7 \pm 12.9\%$ and overlap index $44.9 \pm 13.9\%$), SVM + RBF (DSC $62.4 \pm 11.3\%$ and overlap index $46.4 \pm 12.0\%$) and AdaBoost (DSC $71.8 \pm 11.2\%$ and overlap index $57.1 \pm 13.1\%$).

Table 2 also illustrates that the best performance of our methods is almost the same as that of methods proposed by Loizou et al. [17] (sensitivity 82.7%, specificity 94.2%, DSC 80.7%, and overlap index 69.3%) via a comparison of the results. The best performance of our method, however, is still slightly inferior to that of the method proposed by Destrempe et al. [22], although the numbers of subjects in the two studies are quite different. In [22], 8988 images are used for the experiments and only 29 images are used in our work. In the view of the standard deviation, however, our proposed method with the random forest algorithm has the more stable segmentation performance compared with that in [22] and our method using linear SVM, SVM + RBF, and AdaBoost algorithms. Compared with the results in the paper of Golemati et al. [23], the best performance of our proposed methods is much lower, no matter the sensitivity and specificity, and the standard deviations of both sensitivity and specificity.

Table 3 tabulates the performance metrics of EArea, AEArea, point-to-point distance (D), and Hausdorff distance (HD), as well

as the results in [22]. The best result with our method is still obtained by integrating the random forest algorithm, which contains EArea $-1.02 \pm 18.3\%$, AEArea $14.7 \pm 10.9\%$, D $0.34 \pm 0.10\text{mm}$, and HD $1.75 \pm 1.02\text{mm}$. Compared the best statistical results of discrepancy by our method with those by the proposed method of Destrempe et al. [22], especially in the comparison of standard deviations, the best performance of our proposed method is still inferior to that in [22].

Fig. 9 shows the ROC curves for the proposed method with the four different classification algorithms based on the TPR and false positive rate (FPR). The FPR is calculated when the computerized method wrongly identifies a non-plaque pixel as a plaque pixel. The area under the ROC curve (AUC) is 0.821, 0.846, 0.884, and 0.897 for the linear SVM, SVM + RBF, AdaBoost, and random forest, respectively. It is clear that the largest AUC is obtained by the method using the random forest algorithm, and the AUCs by other three algorithms are also over 0.8.

4.4. The importance of the Auto-context model

In the proposed methods, the auto-context model plays an important role. It can improve the performance of plaque segmentation iteratively. In our work, we set the number of auto-context iterations at 10, which is the same as that in [46,47]. Fig. 10 shows the changes in the sensitivity (TPR), specificity (TNR), DSC, and overlap index by applying the four different classification algorithms with the auto-context model based on the B-mode ultrasound images. The influence of the auto-context model on the other four measures, EArea, AEArea, point-to-point distance (D), and Hausdorff distance (HD), are shown in Fig. 12. It can be seen

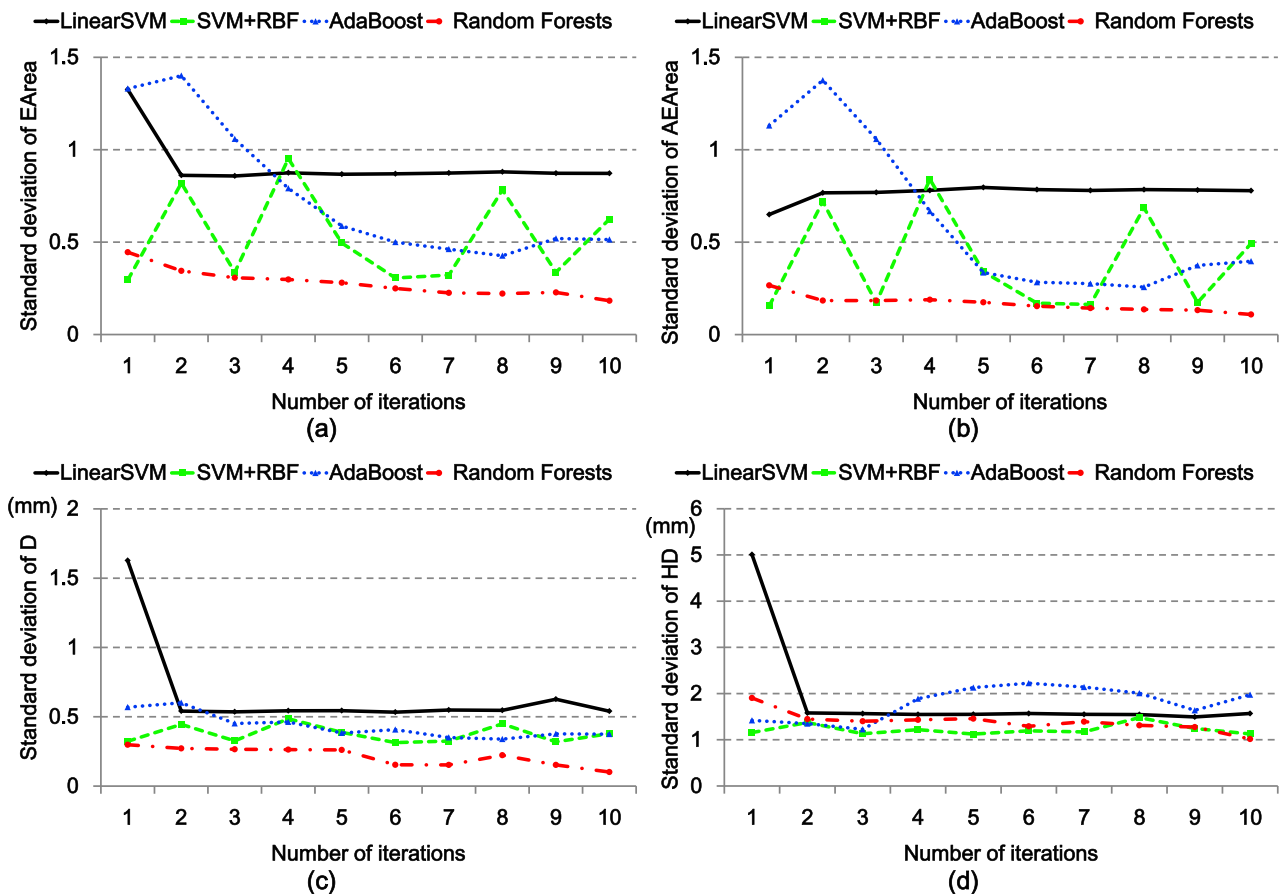


Fig. 13. Changes in the standard deviations of the (a) EArea, (b) AEArea, (c) D, and (d) HD, with iterations, respectively. (For interpretation of the references to color in this figure legend, the reader is referred to the web version of this article.)

that all of the indices are improved with the iterations, except for that using SVM + RBF. Specifically, in the second iteration, all the indices are improved greatly due to the integration of the previously estimated tissue probability maps for guiding the classification. These results demonstrate the importance of using context features for plaque segmentation.

The context features can also help our method become more stable, which can also be clearly observed in Figs. 11 and 13. The standard deviations of the evaluation indices are shown in both figures, which is an important measurement to reflect the stability of the proposed method. With the increase of the number of iterations, the standard deviations become lower and lower, and very close to zero.

Figs. 10 to 13 also show that the method integrating random forest is superior. Among the results from the four different classification algorithms, only that using random forest continues to improve, i.e., all of the eight indices are stably higher and higher, and the standard deviations are moving lower and lower, with iterations. There is no special point on the statistical line of each index by the random forest method, except for that of standard deviations of sensitivity, standard deviations of DSC, and standard deviations of overlap index in iterations 6 and 7.

4.5. Comparisons with other State-of-the-art methods

To further evaluate the performance of our proposed method, we compare the results obtained by our method with several other state-of-the-art plaque segmentation methods on our dataset. We use the methods proposed in [14,17–19,22,24], which can be classified into snake models [17–19], Gamma distribution & NaiveBayes

model [22], and level sets [14,24]. All these methods are implemented in the semi-automatic manner, i.e., the initialization of these methods is based on the manually delineated plaque contour from the Doppler color ultrasound images in the dataset. It is to be noted that a normalization algorithm and speckle reduction filtering [17] are used to preprocess the images.

In Fig. 14, the comparisons of the performance between the state-of-the-art methods and our method are made based on the eight indices: sensitivity, specificity, DSC, overlap, EArea, AEArea, D and HD. It can be seen that our method integrating random forest obtains the best results on almost all the evaluation indices. In Fig. 14(c) and (d), we can see that the results from random forest show the highest coincidence to the manual delineated ground truth, which is illustrated by highest 81.0% average DSC and 68.3% average overlap rate. The best EArea (-0.010) and AEArea (0.147) values (Fig. 14(e) and (f)) show that the plaque boundary obtained by the random forest in our method is the closest to the ground truth. From Fig. 14(e), we find that according to the definition of EArea in [22], most of the methods will underestimate (-) the plaque boundary, except for the Gamma distribution & NaiveBayes model (+0.274). The lowest 1.751 mm HD (in Fig. 14(h)) shows that the random forest can contour the plaque boundary almost the same as the expert's hand contouring.

In comparison with other existing methods, however, the results from random forest in sensitivity, specificity and D show that the method integrated with random forest still can be improved. In Fig. 14(a), Balloon (83.8%), Lai & Chin (82.8%) [17], and LinearSVM (83.0%) return almost the same best values of sensitivity, which are nearly 3% larger than that by random forest (80.4%). For the specificity (Fig. 14(b)), the result from random forest (96.5%) is only

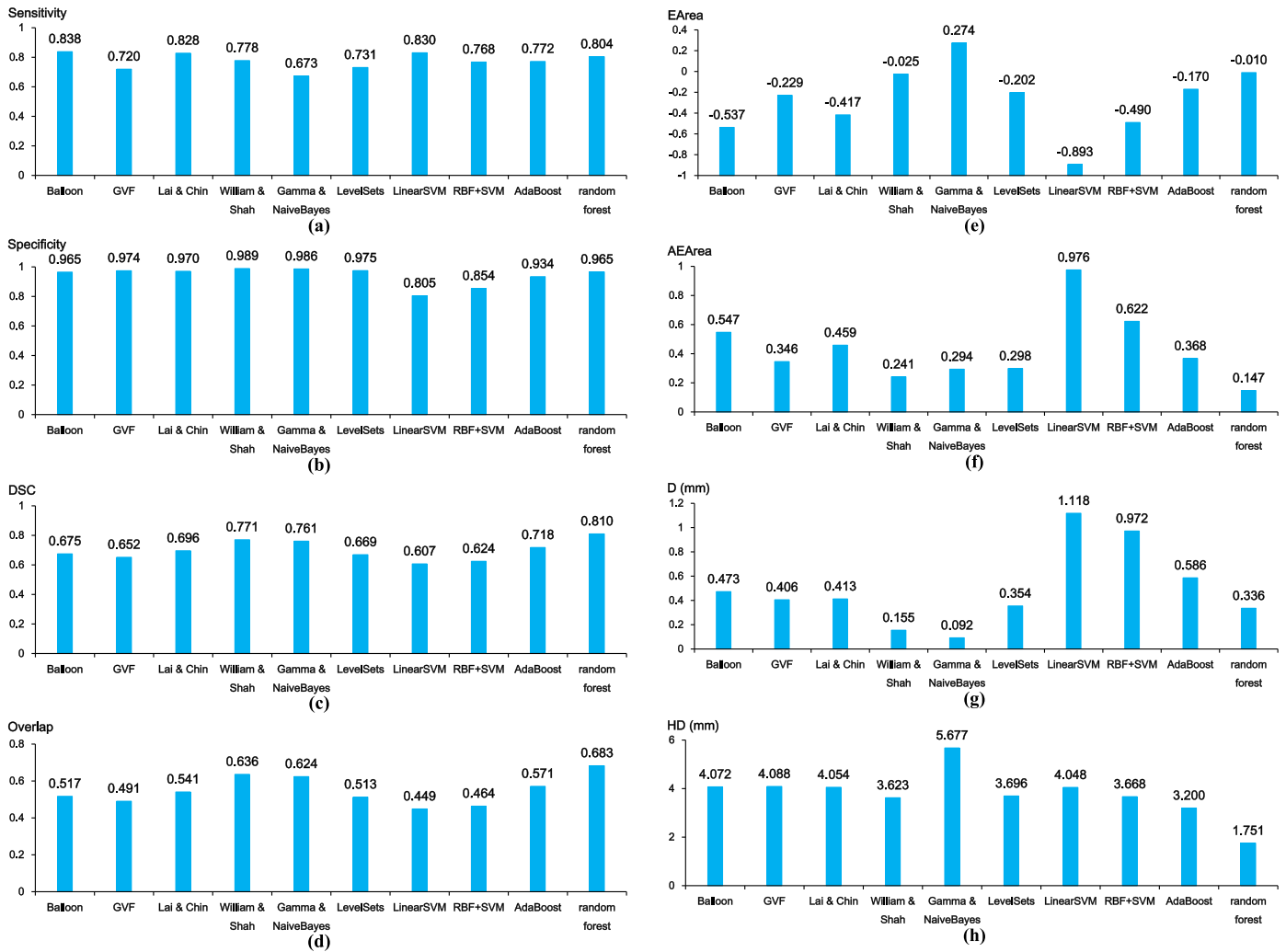


Fig. 14. The comparisons of the performance between the state-of-the-art methods and our proposed method. (a) Sensitivity; (b) Specificity; (c) DSC; (d) Overlap; (e) EArea; (f) AEArea; (g) D; and (h) HD.

higher than those from LinearSVM (80.5%), RBF + SVM (85.4%) and AdaBoost (93.4%). This also demonstrates that the performance of random forest in segmenting the non-plaque region is not better than the existing methods: Balloon (96.5%), GVF (97.4%), Lai & Chin (97.0%), William & Shah (98.9%), Gamma distribution & NaiveBayes model (98.6%), and level sets (97.5%). The D metric in Fig. 14(g) indicates that the point on the plaque boundary by random forest (0.336 mm) is farther away from the nearest point on the manual delineated boundary, compared with the results from William & Shah (0.155 mm) and Gamma distribution & NaiveBayes model (0.092 mm).

The ROC curves based on the TPR and FPR for the existing methods and our proposed methods are shown in Fig. 15. The area under the ROC curve (AUC) for the Balloon is 0.897, GVF 0.846, Lai & Chin 0.894, William & Shah 0.868, Gamma distribution & NaiveBayes model 0.816, level sets 0.849, linear SVM 0.821, SVM + RBF 0.846, AdaBoost 0.884, and random forest 0.897. It can be observed that the AUCs of all the algorithms are over 0.8, and furthermore, the largest AUC (0.897) is obtained by both random forest and the Balloon model.

5. Discussion

In this paper, we have proposed a semi-automatic method for atherosclerotic carotid plaque segmentation in ultrasound images.

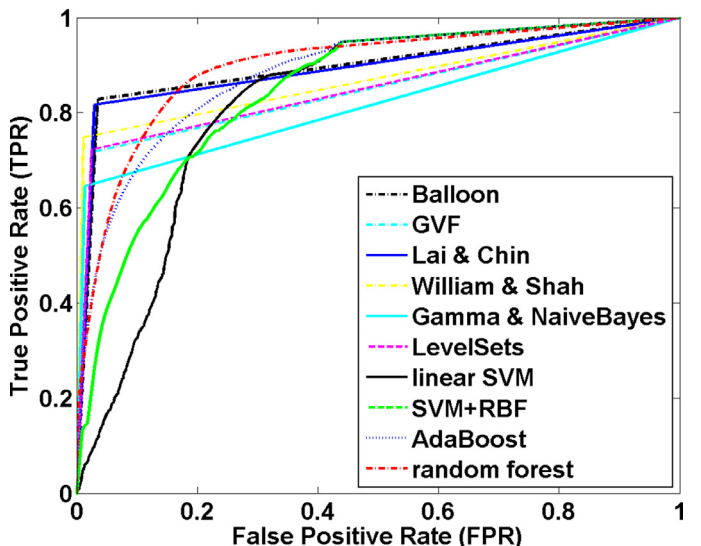


Fig. 15. ROC curves based on the TPR and FPR for the existing methods and proposed methods: Balloon, GVF, Lai & Chin, William & Shah, Gamma distribution & NaiveBayes model, level sets, linear SVM, SVM + RBF, AdaBoost and random forest. (For interpretation of the references to color in this figure legend, the reader is referred to the web version of this article.)

The learning-based algorithm and auto-context model are integrated in our proposed method. Specifically, the learning-based algorithm is employed in three steps in our proposed method, including ROI extraction, candidate plaque area identification and plaque segmentation. Each step is essential and implemented automatically. In our method, the procedures of ROI extraction and candidate plaque area identification can be regarded as the preparations of plaque segmentation. In the plaque segmentation process, the importance of the auto-context model is demonstrated by improving the accuracy of the results and making the proposed method more and more robust and stable.

Compared with the works of other researchers, however, such as [22], there are three limitations in our study: (1) The number of images is limited. In [22], a total of 8988 images with carotid arteries stenosis are included. In our study, only 29 B-mode ultrasound images are validated. To overcome this limitation, in our experiments, we detect over 150,000 samples from 29 images and use the pixel level classification method. In our method, each extracted pixel is treated as the training or testing sample. (2) For the learning-based segmentation method, more time is spent in the training stage. In Step I, the average training time is 5 min. In Step II, the training time is 21 min, and 40 min are spent in Step III. In a word, approximately 66 min are taken to train a classification model in each auto-context iteration, i.e., over 7 h ($5\text{ min} + 21\text{ min} + 40\text{ min} \times 10 = 426\text{ min} \geq 7\text{ h}$) are spent building a complete plaque segmentation model in the training stage. We also compute the time in the testing stage. For a new input image, our method should take approximately 6 min to finish the plaque segmentation, which is also time-consuming, compared to 38 s in [22]. The main difference is the usage of the GPU implementation, which can greatly improve the computational speed in image processing [52]. (3) The main limitation is the lack of a special ultrasound image reader. In the database used here, the plaques of type II, III, and IV are outlined. Although the fibrous caps of the plaques are easily identified, differences among the plaques still exist. Some plaques are very bright, while others are darker. Because there is no special image reader to sort the plaques into three categories according to the types of plaque, we treat all of the plaques with different types as the same lesion tissue in our work, i.e., the region of positive samples. This affects the performance of the trained classifiers. Therefore, not all the segmentation results are satisfactory compared to the ground truth.

Considering the computational speed, currently, our proposed method can only be used offline or for preoperative preparation and not in real time. If the population of patients is too large and experts cannot give advice in time, experts can record the images of patients on the server and implement our proposed segmentation method for atherosclerotic carotid plaque. After segmenting atherosclerotic carotid plaque on the image, an expert can assess the risk of stroke by measuring the carotid plaque burden in the patient. Then, expert can provide accurate advice and develop an accurate treatment plan without excessive manual operations on the ultrasound image. Furthermore, before surgical treatment (i.e., carotid endarterectomy (CEA)) on the patient, surgeons can accurately segment the plaque and measure the size of the plaque in the ultrasound image with our proposed method. This is helpful to assess potential surgical difficulties and risks in advance.

The major contribution of our work is that our proposed method integrates learning-based algorithms and an auto-context model to segment the atherosclerotic carotid plaque semi-automatically in the whole ultrasound image, and achieves similar performance as the existing methods. In our future work, the proposed method will be improved, e.g., through the improvement of algorithms used in our method, computational speed, etc. Furthermore, we will collect more useful data to optimize the training classification model, which will be helpful to improve the perfor-

mance of our plaque segmentation method. Because the plaques used in our work are of three different types, we will establish three different classification models for segmenting each corresponding type of plaque, with the help of a special ultrasound image reader. Additionally, the new collected data will be of the three different types of plaque, which will improve the performance of the three different plaque segmentation models.

6. Conclusion

We have proposed a novel integrated framework for atherosclerotic carotid plaque segmentation in the B-mode ultrasound image. Our proposed method can segment the plaque regions from the entire images. Specifically, the proposed method integrating the random forest and an auto-context model can effectively segment the plaque, combining with the extracted features from ultrasound images and also the iteratively estimated probability maps. Experimental results on the database show that the performance of our method using random forest is almost the same as that of the existing methods and the proposed method will be helpful for accurately segmenting the plaque and measuring the carotid plaque burden in the ultrasound image. In our future work, we will further improve our method, validate our proposed method on more patient subjects and classify or identify the plaque type in the ultrasound image.

References

- [1] D. Mozaffarian, E.J. Benjamin, A.S. Go, D.K. Arnett, M.J. Blaha, M. Cushman, S.R. Das, S. de Ferranti, J.-P. Després, H.J. Fullerton, Executive Summary, Heart disease and stroke statistics—2016 update: a report from the American heart association, *Circulation* 133 (2016) 447–454.
- [2] C. Bogatzki, D.G. Hackam, A.I. Mcleod, J.D. Spence, Secular trends in ischemic stroke subtypes and stroke risk factors, *Stroke* 45 (2014) 3208–3213.
- [3] J.D. Spence, Measurement of carotid plaque burden, *JAMA Neurol.* 72 (2015) 383–384.
- [4] R.B. Singh, S.A. Mengi, Y.J. Xu, A.S. Arneja, N.S. Dhalla, Pathogenesis of atherosclerosis: a multifactorial process, *Exp. Clin. Cardiol.* 7 (2002) 40.
- [5] C.K. Zarins, C. Xu, S. Glagov, Atherosclerotic enlargement of the human abdominal aorta, *Atherosclerosis* 155 (2001) 157–164.
- [6] K.P. Economopoulos, T.N. Sergentanis, G. Tsivgoulis, A.D. Mariolis, C. Stefanadis, Carotid artery stenting versus carotid endarterectomy a comprehensive meta-analysis of short-term and long-term outcomes, *Stroke* 42 (2011) 687–692.
- [7] S. Glagov, E. Weisenberg, C.K. Zarins, R. Stankunavicius, G.J. Kolettis, Compensatory enlargement of human atherosclerotic coronary arteries, *New Engl. J. Med.* 316 (1987) 1371–1375.
- [8] A.M.F. Santos, R.M. Dos Santos, P.M.A. Castro, E. Azevedo, L. Sousa, J.M.R. Tavares, A novel automatic algorithm for the segmentation of the lumen of the carotid artery in ultrasound B-mode images, *Expert Syst. Appl.* 40 (2013) 6570–6579.
- [9] R.M. Menchón-Lara, M.C. Bastida-Jumilla, J. Morales-Sánchez, J.L. Sancho-Gómez, Automatic detection of the intima-media thickness in ultrasound images of the common carotid artery using neural networks, *Med. Bio. Eng. Comput.* 52 (2014) 169–181.
- [10] T. Wannarong, G. Parraga, D. Buchanan, A. Fenster, A.A. House, D.G. Hackam, J.D. Spence, Progression of carotid plaque volume predicts cardiovascular events, *Stroke* 44 (2013) 1859–1865.
- [11] J.D. Spence, Approaching automated 3-dimensional measurement of atherosclerotic plaque volume, *J. Am. College Cardiol.* 70 (2017) 314–317.
- [12] P. Abolmaesumi, M.R. Sirouspour, S.E. Salcudean, Real-time extraction of carotid artery contours from ultrasound images, in: Proceedings of the 13th IEEE Symposium on Computer-Based Medical Systems (CBMS'00) (CBMS '00), IEEE, 2000, pp. 181–186.
- [13] J. Guerrero, S.E. Salcudean, J.A. Mcewen, B.A. Masri, S. Nicolaou, Real-time vessel segmentation and tracking for ultrasound imaging applications, *IEEE Trans. Med. Imaging* 26 (2007) 1079–1090.
- [14] E. Ukwatta, J. Yuan, D. Buchanan, B. Chiu, J. Awad, W. Qiu, G. Parraga, A. Fenster, Three-dimensional segmentation of three-dimensional ultrasound carotid atherosclerosis using sparse field level sets, *Med. Phys.* 40 (2013) 384–389.
- [15] A.K. Hamou, M.R. El-Sakka, A novel segmentation technique for carotid ultrasound images, in: IEEE International Conference on Acoustics, 2004, pp. 521–524.
- [16] A.R. Abdel-Dayem, M.R. El-Sakka, A novel morphological-based carotid artery contour extraction, in: Canadian Conference on Electrical & Computer Engineering, 1874, 2004, pp. 1873–1876.
- [17] C.P. Loizou, C.S. Pattichis, M. Pantziaris, A. Nicolaides, An integrated system for the segmentation of atherosclerotic carotid plaque, *IEEE Trans. Inf. Technol. Biomed.* 11 (2007) 661–667.

- [18] J. Gill, H. Ladak, D. Steinman, A. Fenster, Segmentation of ulcerated plaque: a semi-automatic method for tracking the progression of carotid atherosclerosis, in: Engineering in Medicine and Biology Society, 2000. Proceedings of the 22nd Annual International Conference of the IEEE, IEEE, 2000, pp. 669–672.
- [19] L.D. Cohen, On active contour models and balloons, *CVGIP: Image Underst.* 53 (1991) 211–218.
- [20] M.-H.R. Cardinal, J. Meunier, G. Soulez, É. Thérasse, G. Cloutier, Intravascular ultrasound image segmentation: a fast-marching method, in: International Conference on Medical Image Computing and Computer-Assisted Intervention, Springer, 2003, pp. 432–439.
- [21] D. Buchanan, I. Gyacskov, E. Ukwatta, T. Lindenmaier, A. Fenster, G. Parraga, Semi-automated segmentation of carotid artery total plaque volume from three dimensional ultrasound carotid imaging, in: SPIE Medical Imaging, International Society for Optics and Photonics, 2012, p. 17.
- [22] F. Destrempe, J. Meunier, M.F. Giroux, G. Soulez, Segmentation of plaques in sequences of ultrasonic b-mode images of carotid arteries based on motion estimation and a Bayesian model, *IEEE Trans. Biomed. Eng.* 58 (2011) 2202–2211.
- [23] S. Golemati, J. Stoitsis, E.G. Sifakis, T. Balkizas, K.S. Nikita, Using the Hough transform to segment ultrasound images of longitudinal and transverse sections of the carotid artery, *Ultrasound Med. Bio.* 33 (2007) 1918–1932.
- [24] J. Cheng, H. Li, F. Xiao, A. Fenster, X. Zhang, X. He, L. Li, M. Ding, Fully automatic plaque segmentation in 3-d carotid ultrasound images, *Ultrasound Med. Bio.* 39 (2013) 2431–2446.
- [25] A. Gastounioti, A. Sotiras, K.S. Nikita, N. Paragios, Graph-based motion-driven segmentation of the carotid atherosclerotic plaque in 2d ultrasound sequences, in: International Conference on Medical Image Computing and Computer-Assisted Intervention, Springer, 2015, pp. 551–559.
- [26] S.C.H.V.D. Oord, Z. Akkus, J.E.R.V. Lennep, J.G. Bosch, A.F.W.V.D. Steen, E.J.G. Sijsbrandts, A.F.L. Schinkel, Assessment of subclinical atherosclerosis and intraplaque neovascularization using quantitative contrast-enhanced ultrasound in patients with familial hypercholesterolemia, *Atherosclerosis* 231 (2013) 107–113.
- [27] Z. Akkus, D.D.B. Carvalho, S.C.H.V.D. Oord, A.F.L. Schinkel, W.J. Niessen, N.D. Jong, A.F.W.V.D. Steen, S. Klein, J.G. Bosch, Fully automated carotid plaque segmentation in combined contrast-enhanced and b-mode ultrasound, *Ultrasound Med. Bio.* 41 (2015) 517–531.
- [28] C. Loizou, Despeckle filtering algorithms and software for ultrasound imaging, *Synth. Lect. Algorithms Software Eng.* 1 (2008) 166.
- [29] G.N. Yannakakis, S. Member, J. Levine, J. Hallam, M. Papageorgiou, Performance, robustness and effort cost comparison of machine learning mechanisms in FlatLand, in: In Proceedings Of The 11th Mediterranean Conference On Control And Automation Med'03, IEEE, 2003.
- [30] R. Biswas, L. Blackburn, J. Cao, R. Essick, K.A. Hodge, E. Katsavounidis, K. Kim, Y.M. Kim, E.O.L. Bigot, C.H. Lee, Application of machine learning algorithms to the study of noise artifacts in gravitational-wave data, *Phys. Rev. D Particles Fields* 88 (2013).
- [31] M. Loog, B. Ginneken, Segmentation of the posterior ribs in chest radiographs using iterated contextual pixel classification, *Med. Imaging, IEEE Trans.* 25 (2006) 602–611.
- [32] Z. Tu, X. Bai, Auto-context and its application to high-level vision tasks and 3d brain image segmentation, *Pattern Anal. Mach. Intell., IEEE Trans.* 32 (2010) 1744–1757.
- [33] I.N. Staikov, M. Arnold, H.P. Mattle, L. Remonda, M. Sturzenegger, R.W. Baumgartner, G. Schroth, Comparison of the ecst, cc, and nasct grading methods and ultrasound for assessing carotid stenosis. European carotid surgery trial. North American symptomatic carotid endarterectomy trial, *J. Neurology* 247 (2000) 681–686.
- [34] A. Nicolaides, M. Sabetai, S. Kakkos, S. Dhanjil, The asymptomatic carotid stenosis and risk of stroke (ACRS) study, *International Angiology* 22 (2003) 263.
- [35] C. Loizou, C. Pattichis, R. Istepanian, M. Pantziaris, A. Nicolaides, Atherosclerotic carotid plaque segmentation, in: Engineering in Medicine and Biology Society, 2004. IEMBS'04. 26th Annual International Conference of the IEEE, IEEE, 2004, pp. 1403–1406.
- [36] R. Achanta, A. Shaji, K. Smith, A. Lucchi, P. Fua, S. Süstrunk, SLIC superpixels compared to state-of-the-art superpixel methods, *IEEE Trans. Pattern Anal. Mach. Intell.* 34 (2012) 2274–2282.
- [37] K.S. Choi, K.W. Oh, Fast simple linear iterative clustering by early candidate cluster elimination, in: Iberian Conference Pattern Recognition and Image Analysis, Ibpria, 2015, pp. 579–586.
- [38] Y. Freund, R.E. Schapire, A desicion-theoretic generalization of on-line learning and an application to boosting, in: Computational Learning Theory, Springer, 1995, pp. 23–37.
- [39] J. Krejza, M. Arkuszewski, S.E. Kasner, J. Weigle, A. Ustymowicz, R.W. Hurst, B.L. Cucchiara, S.R. Messe, Carotid artery diameter in men and women and the relation to body and neck size, *Stroke* 37 (2006) 1103–1105.
- [40] T. Nilsson, S. Segstedt, Å.R. Ahlgren, S. Ricci, G. Östling, P. Tortoli, J. Nilsson, T. Jansson, H.W. Persson, M. Cinthio, A robust and fast method for arterial lumen diameter and intima-media thickness measurements, in: Ultrasonics Symposium, 2013, pp. 1678–1681.
- [41] C.-W. Hsu, C.-J. Lin, A comparison of methods for multiclass support vector machines, *Neural Networks, IEEE Trans.* 13 (2002) 415–425.
- [42] R. Gilad-Bachrach, A. Navot, N. Tishby, Margin based feature selection-theory and algorithms, in: Proceedings of the twenty-first international conference on Machine learning, ACM, 2004, p. 43.
- [43] L. Breiman, Random forests, *Mach. Learn.* 45 (2001) 5–32.
- [44] Y. Qi, Random forest for bioinformatics, in: Ensemble Machine Learning, Springer, 2012, pp. 307–323.
- [45] A. Criminisi, J. Shotton, Decision Forests For Computer Vision and Medical Image Analysis, Springer, 2013.
- [46] L. Wang, Y. Gao, S. Feng, G. Li, J.H. Gilmore, W. Lin, D. Shen, LINKS: learning-based multi-source integration framework for segmentation of infant brain images, *Neuroimage* 108 (2015) 160–172.
- [47] C. Qian, L. Wang, Y. Gao, A. Yousef, X. Yang, A. Oto, D. Shen, Vivo MRI based prostate cancer localization with random forests and auto-context model, *Computerized Medical Imaging and Graphics* 52 (2016) 44–57.
- [48] T. Fawcett, An introduction to ROC analysis, *Pattern Recognit. Lett.* 27 (2006) 861–874.
- [49] S. Andrews, G. Hamarneh, Multi-region probabilistic dice similarity coefficient using the aitchison distance and bipartite graph matching (2015) arXiv:1509.07244.
- [50] F. Molinari, W. Liboni, E. Pavanelli, P. Giustetto, Accurate and automatic carotid plaque characterization in contrast enhanced 2-D ultrasound images, in: Engineering in Medicine and Biology Society, 2007. EMBS 2007. International Conference of the IEEE, 2007, pp. 335–338.
- [51] D.P. Huttenlocher, G.A. Klanderman, W.J. Rucklidge, Comparing images using the Hausdorff distance, *IEEE Trans. Pattern Anal. Mach. Intell.* 15 (1993) 850–863.
- [52] M. Wang, B. Wang, Q. He, X. Liu, K. Zhu, M. Wang, B. Wang, Q. He, X. Liu, K. Zhu, Analysis of GPU parallel computing based on Matlab (2015) arXiv:1505.06561.